Photonics-enabled balanced Hartley architecture for broadband image-reject microwave mixing

DAN ZHU, WENJUAN CHEN, AND SHILONG PAN[*]

Key Laboratory of Radar Imaging and Microwave Photonics, Ministry of Education, Nanjing University of Aeronautics and Astronautics, Nanjing 210016, China
*pans@nuaa.edu.cn

Abstract: Conventional image-reject mixing based on Hartley and Weaver architectures cannot deal with the mixing spurs generated by the nonlinearity of the mixer, leading to a fundamental restriction on the instantaneous bandwidth and frequency tuning range. This paper proposes and demonstrates a new architecture for broadband image-reject mixing enabled uniquely by photonics. The RF signal and the electrical LO signal are converted into the optical domain and are then launched into the signal and LO ports of a 90-degree optical hybrid, respectively. The optical hybrid coupler introduces 0, π, $\pi/2$ and $3\pi/2$ phase shifts to the input signals, so a new dimension for additional balanced detection is enabled, which can dramatically remove the undesirable mixing spurs and the common-mode noises. As a result, the proposed architecture suppresses the downconverted image and the nonlinear mixing spurs simultaneously, enabling a truly wideband microwave frequency mixer. A theoretical and experimental investigation is performed. More than 60-dB image rejection and mixing spur suppression is achieved over a 40-GHz working frequency range.

1. Introduction

Frequency downconverter is an essential part in almost all the RF information systems [1–3], by which a radio frequency (RF) signal at ω_{RF} is mixed with a local oscillator (LO) signal at ω_{LO} to generate an intermediate frequency (IF) signal at $\omega_{IF} = |\omega_{RF}-\omega_{LO}|$ for further processing in low-frequency receivers. One critical problem associated with the downconverters is the image interference resulted from the unwanted frequency component that has a frequency ω_{IM} above or below the LO frequency by an amount equal to the IF frequency ω_{IF}, i.e., $|\omega_{LO}-\omega_{IM}| = \omega_{IF}$. To suppress the image interference without employing a pre-filter, image-reject mixers (IRMs) based on phase-cancellation technique known as the Hartley architecture and the Weaver architecture were proposed in the 1980s [4]. Figure 1 shows the schematic diagram of the Hartley architecture based IRM. The key is to introduce a pair of quadrature LO (or RF) signals, which mix with the RF (or LO) signals to generate two quadrature IF outputs. The two IF signals are then combined by a quadrature hybrid, which introduces an additional $\pi/2$-phase difference to make the downconverted image out of phase and the wanted IF signals in phase. As a result, the wanted IF signals are enhanced, while the downconverted image at the same band is canceled. The Hartley architecture was further evolved to Weaver architecture [4], using a second quadrature mixing stage to solve the phase mismatch problem in the $\pi/2$ phase shift network. In addition, in order to break the electronic bottleneck [5], many photonics-based approaches were previously reported to extend the working frequency range and bandwidth [5–15], but almost all of them were implemented based on the Hartley architecture.

Both the Hartley and Weaver architectures, however, can only eliminate the downconverted image, which are incapable to cope with the RF/LO leakages and mixing spurs generated by the nonlinearity of the mixer (for example, the mixing component between the RF and image) [4]. Since many of these undesired components are very close to or even

overlap with the wanted IF signal, the existence of them lays a fundamental restriction on the instantaneous bandwidth and frequency tuning range of the RF systems. With the fast development of wideband systems, broadband image-reject mixing becomes a key requirement for 5G and beyond wireless communications, ultrahigh-capacity satellite payloads, electronic warfare, and multifunctional radars.
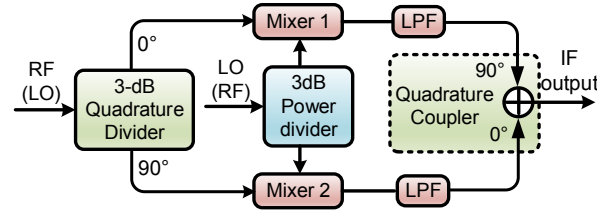

Fig. 1. The schematic diagram of the image-reject mixer based on the Hartley architecture [4], LPF: low pass filter.

In this paper, we propose a new image-reject mixing architecture that can simultaneously realize high rejection of the linear image and leakage components and significant suppression of the nonlinear mixing spurs over multi-octave frequency range. The key to realizing such an architecture is the fact that the hybrid coupler implemented in the optical domain can simultaneously introduce precise 0, π, $\pi/2$ and $3\pi/2$ phase shifts to the input signals [16,17], so a new dimension for additional balanced detection is enabled, which can remove the undesirable mixing spurs. A theoretical and experimental investigation is performed on the low-spur-level IRM based on the proposed balanced Hartley architecture. More than 60-dB image and mixing spur suppression is achieved over a frequency range of 40 GHz. Performance of the mixing spur rejection ratio versus the LO power is also investigated.
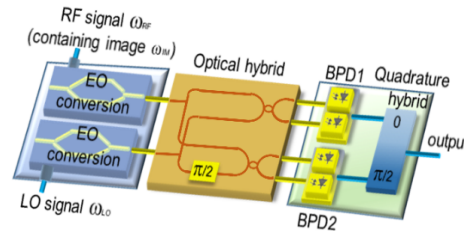
2. Principle

Fig. 2. The schematic diagram of the proposed balanced Hartley architecture for broadband image-reject microwave mixing.

The schematic diagram of the proposed balanced Hartley architecture for broadband image-reject microwave mixing is shown in Fig. 2. The RF signal at ω_{RF} (containing the image at ω_{IM}) and the electrical LO signal of ω_{LO} are converted into the optical domain, and are then injected into the signal and LO ports of a 90-degree optical hybrid, respectively. The frequency of the optical carrier is set to be ω_c. The optical fields of the optically-carried RF signal (containing the image) and the LO can be written as

$$
\begin{aligned}
E_{RF}(t) &\propto a_{-1}\exp j(\omega_c t - \omega_{RF}t - \theta_{RF}) + b_{-1}\exp j(\omega_c t - \omega_{IM}t - \theta_{IM}) \\
&\quad + a_0 \exp j(\omega_c t) \\
&\quad + a_1 \exp j(\omega_c t + \omega_{RF}t + \theta_{RF}) + b_1 \exp j(\omega_c t + \omega_{IM}t + \theta_{IM}) \\
E_{LO}(t) &\propto d_1 \exp j(\omega_c t + \omega_{LO}t + \theta_{LO})
\end{aligned}
\tag{1}
$$

where a_{-1}, a_1, a_0, b_{-1}, b_1 represent the amplitudes of the corresponding spectral components in the optically-carried RF signal, and d_1 is the amplitude of the optically-carried LO. The optical hybrid introduces 0, π, $\pi/2$ and $3\pi/2$ phase shifts to the optical LO, leading to two in-phase ($I_1 \propto E_{RF} + E_{LO}$ and $I_2 \propto E_{RF}-E_{LO}$) and two quadrature ($Q_1 \propto E_{RF} + jE_{LO}$ and $Q_2 \propto E_{RF}-jE_{LO}$) optical outputs. The two in-phase (I_1 and I_2) and two quadrature (Q_1 and Q_2) optical signals are sent into two balanced photodetectors (BPDs), respectively. Through optical to electrical conversion, the electrical components generated from I_1 and I_2 (or Q_1 and Q_2) at $\omega_{IF} = |\omega_{RF}-\omega_{LO}|$, $|\omega_{LO}-\omega_{IM}|$, $\omega_{RF} + \omega_{LO}$, $\omega_{LO} + \omega_{IM}$ and ω_{LO} (the LO leakage) are out of phase, while the RF leakages and mixing spurs at ω_{RF}, ω_{IM}, $2\omega_{IF} = |\omega_{RF}-\omega_{IM}|$, $2\omega_{RF}$, $2\omega_{IM}$, and $\omega_{RF} + \omega_{IM}$ are in phase. With an additional π-phase difference introduced by the BPDs, the electrical outputs at the two BPDs are given by

$$
\begin{aligned}
i_1 &\propto I_1^* I_1 - I_2^* I_2 \\
&= 4a_1 d_1 \cos(\omega_{RF}t - \omega_{LO}t + \theta_{RF} - \theta_{LO}) + 4b_1 d_1 \cos(\omega_{LO}t - \omega_{IM}t + \theta_{LO} - \theta_{IM}) \\
&\quad + 4a_{-1} d_1 \cos(\omega_{LO}t + \omega_{RF}t + \theta_{LO} + \theta_{RF}) + 4b_{-1} d_1 \cos(\omega_{LO}t + \omega_{IM}t + \theta_{LO} + \theta_{IM}) \\
&\quad + 4a_0 d_1 \cos(\omega_{LO}t + \theta_{LO}) \\
i_Q &\propto Q_1^* Q_1 - Q_2^* Q_2 \\
&= 4a_1 d_1 \sin(\omega_{RF}t - \omega_{LO}t + \theta_{RF} - \theta_{LO}) - 4b_1 d_1 \sin(\omega_{LO}t - \omega_{IM}t + \theta_{LO} - \theta_{IM}) \\
&\quad - 4a_{-1} d_1 \sin(\omega_{LO}t + \omega_{RF}t + \theta_{LO} + \theta_{RF}) - 4b_{-1} d_1 \sin(\omega_{LO}t + \omega_{IM}t + \theta_{LO} + \theta_{IM}) \\
&\quad - 4a_0 d_1 \sin(\omega_{LO}t + \theta_{LO})
\end{aligned}
\tag{2}
$$

As can be seen, the RF leakages at ω_{RF} and ω_{IM}, and the mixing spurs at $2\omega_{IF} = |\omega_{RF}-\omega_{IM}|$, $2\omega_{RF}$, $2\omega_{IM}$, and $\omega_{RF} + \omega_{IM}$ are eliminated. In addition, the two electrical outputs of i_I and i_Q are quadrature because the 90-degree optical hybrid also introduces a quadrature phase of the optical LO for the in-phase and the quadrature optical outputs (i.e., I_1 and Q_1, I_2 and Q_2). By combining i_I and i_Q using an electrical hybrid, an additional $\pi/2$-phase difference will be introduced, so the output can be expressed as

$$
\begin{aligned}
i &= i_I \angle 0 + i_Q \angle \tfrac{\pi}{2} \\
&\propto 8a_1 d_1 \cos(\omega_{RF}t - \omega_{LO}t + \theta_{RF} - \theta_{LO})
\end{aligned}
\tag{3}
$$

From Eq. (3), the downconverted image at $|\omega_{LO}-\omega_{IM}|$ and the mixing spurs at $\omega_{RF} + \omega_{LO}$, $\omega_{LO} + \omega_{IM}$ and the LO leakage at ω_{LO} are removed. Only the desired IF signal at $\omega_{IF} = |\omega_{RF}-\omega_{LO}|$ is left. In this way, a photonics-based IRM with mixing spurs largely suppressed is realized. Note that the suppression of the image and the mixing spurs is not determined by the amplitudes of the optical carrier and sidebands, indicating that the modulation scheme of the optical RF signal can be arbitrary. The introduced $\pi/2$ and $3\pi/2$, π-phase shifts have important effects with the system performance. In order to achieve excellent performance, precise phase shifts should be provided. In addition, since the required phase differences are realized through photonic techniques, the consistencies of the required phases are guaranteed over a wide RF frequency range, ensuring the large suppression of the image and the mixing spurs within broad bandwidth.

3. Experimental results and discussions

An experiment based on the scheme shown in Fig. 2 is carried out. An optical carrier with a wavelength of 1550.5 nm and a power of 16 dBm is generated from an LD (Teraxion PS-NLL-1550.52-80-04) and then split into two parts with equal powers. A Mach-Zehnder modulator (MZM) with a bandwidth of 40 GHz and a half-wave voltage of less than 4 V is incorporated in each branch to realize the electrical to optical conversion. A 90° optical hybrid (Kylia COH28) is used to combine the two paths, which outputs four signals to two BPDs. The BPDs (BPDV2150R-VF-FP) have a bandwidth of 40 GHz and a responsivity of

0.53 A/W. The optical spectrum is measured by an optical spectrum analyzer (OSA, YOKOGAWA AQ6370C) with a resolution of 0.02 nm, and the electrical spectrum is observed by an electrical spectrum analyzer (ESA, R&SFSV40) with a frequency range of 10 Hz-40 GHz. In addition, the electrical waveforms are observed by a 32-GHz digital oscilloscope (Agilent DSO-X 92504A).

The modulation formats of the optical RF signal (containing the image) and the LO signal are both set to be the carrier-suppressed single sideband (CS-SSB) modulation. An optical filter is inserted in each branch to remove the undesired sidebands. The LO signal is fixed at 15 GHz with a power of 12 dBm, and the RF signal has a power of 9 dBm and a frequency swept from 15.1 to 20 GHz with a step of 100 MHz. Figure 3 shows the electrical spectra (dashed line) of the IF signals downconverted from the RF signals, which have a power of ~-25 dBm. Then, the RF signal is switched to the image frequency (from 14.9 to 10 GHz). Its power is also fixed at 9 dBm. The downconverted images are shown as the solid lines in Fig. 3. As can be seen, an image rejection ratio of 60 dB can be guaranteed for the whole 5-GHz range.
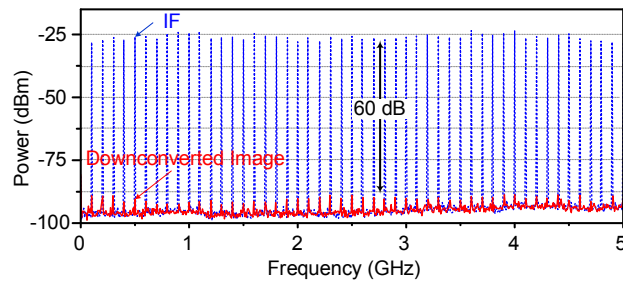

Fig. 3. The electrical spectra of the IF signals from the proposed IRM when the frequency of the RF signal is swept from 15.1 to 20 GHz (dashed line). The solid line denotes the case when the RF signal is switched to the corresponding image.

Then the RF signal and the image are simultaneously injected into the system. Figure 4(a) shows the results using the microwave photonic IRM based on the Hartley architecture [13], i.e., only single-end detection is applied. A mixing spur at $2\omega_{IF} = |\omega_{RF}-\omega_{IM}|$ (red solid line) is generated, which is very close to the downconverted signal at ω_{IF}. If the microwave photonic IRM based on the proposed balanced Hartley architecture is applied, as shown in Fig. 4(b), the undesired mixing spurs are suppressed by more than 60 dB over the whole 5-GHz tuning range.
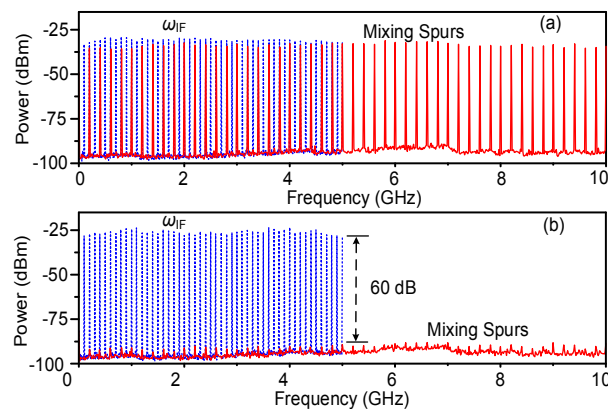

Fig. 4. The electrical spectra of the mixing results from the scheme using (a) the Hartley architecture and (b) the proposed balanced Hartley architecture, when the RF signal with a frequency sweeping from 15.1 to 20 GHz and the corresponding image are introduced to the system.

Figure 5 shows the output mixing results over 0-40 GHz range for the scheme without and with the balanced detection when the RF signal is tuned from 16 to 29 GHz with a step of 1 GHz (containing the corresponding image) while the LO signal is fixed at 15 GHz. For the scheme using the conventional Hartley architecture, the mixing spurs overlap with the wanted IF components, as shown in Fig. 5(a). By using the proposed balanced Hartley architecture, a large suppression of the mixing spurs is ensured, as shown in Fig. 5(b).
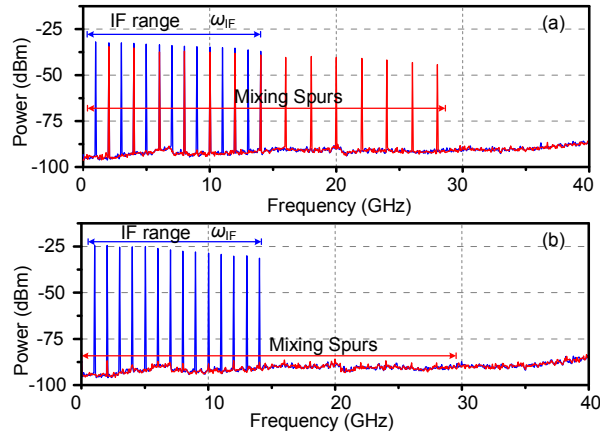

Fig. 5. The electrical spectra of the mixing results from the scheme using (a) the Hartley architecture and (b) the proposed balanced Hartley architecture, when the RF signal with a frequency sweeping from 16 to 29 GHz and the corresponding image are introduced to the system.

Figure 6 shows the image and mixing spur suppression ratio when the RF signal is tuned from 4 to 40 GHz. The LO frequency is selected to let the IF frequency fixed at 1.5 GHz. By using the conventional Hartley architecture, the image can be suppressed by more than 60 dB, while the mixing spurs suppression ratio is <5 dB. By using the proposed balanced Hartley architecture, both the image and the mixing spurs are suppressed by more than 60 dB among the whole tuning range, as shown in Fig. 6(b). The fluctuation of the image/mixing spurs suppression ratio is mainly due to the deviation of the introduced phase shifts and the environment effects. The typical value of the phase shift deviation of the 90-degree optical hybrid used in the experiment is ± 2 degree. By using devices having more accurate phase and amplitude responses, the system performance can be further improved.
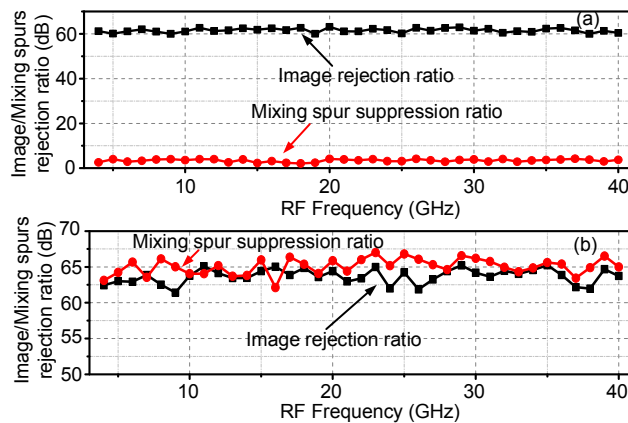

Fig. 6. The rejection ratio of the image/mixing spurs as a function of the RF frequency using (a) the Hartley architecture and (b) the proposed balanced Hartley architecture.

The mixing spur rejection ratio versus the LO power is also investigated. The frequencies of the RF signal and the image are set to be 16.5 and 13.5 GHz, respectively, and the LO frequency is 15 GHz. The power of the RF signal is fixed at 10 dBm, while the LO power is increased from −10 to 10 dBm. As can be seen from Fig. 7, the mixing spur suppression ratio increases linearly with the LO power for both the two schemes. As compared with the conventional Hartley architecture, for all the conditions, about 60-dB improvement of the mixing spur suppression ratio is achieved using the proposed balanced Hartley architecture.
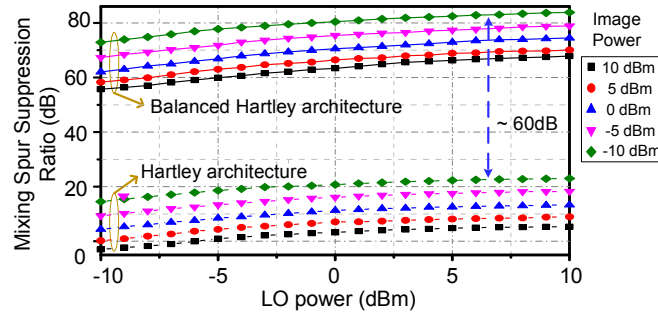

Fig. 7. The mixing spur suppression ratio versus the LO power for the Hartley architecture and the proposed balanced Hartley architecture.
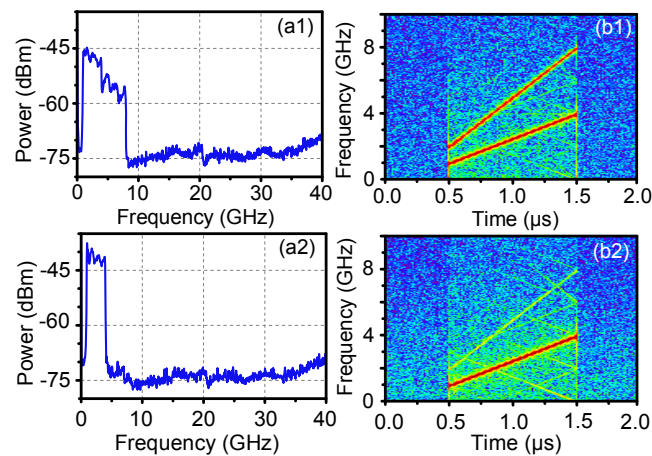

Fig. 8. (a) The electrical spectra and (b) the instantaneous frequency-time diagram of the wideband downconverted signals using the scheme based on (1) the Hartley architecture and (2) the proposed balanced Hartley architecture.

The above measurements are performed based on single- or dual-frequency input, which can only form very few mixing spurs. Figure 8 shows the case when a RF signal and its image with broad instantaneous bandwidth are introduced. The RF signal is a linearly frequency-modulated (LFM) signal with an instantaneous bandwidth of 3 GHz centered at 16.5 GHz, and the LO signal has a frequency of 14 GHz and a power of 10 dBm. The corresponding image has an instantaneous frequency of 10-13 GHz. By injecting the RF signal and the image simultaneously, the mixing results from the scheme using the Hartley architecture are shown in Figs. 8(a1) and 8(b1). As can be seen, the mixing spur (2-8 GHz) overlaps with the downconverted IF signal (1-4 GHz) which obviously cannot be removed by filtering. Figures 8(a2) and 8(b2) show the output of the proposed scheme. As can be seen, a clean IF signal centered at 2.5 GHz with a 3-GHz bandwidth is obtained with the image and mixing spurs largely suppressed. In addition, thanks to the balanced detection, all the output optical power of the 90° optical hybrid can be used while the scheme based on the Hartley architecture can only apply two of the four optical channels. As a result, a 6-dB power gain of the IF signal

can be observed in Fig. 8(a2). Thus, using the proposed architecture, a broad instantaneous bandwidth is guaranteed with an improved conversion efficiency.

In order to verify that the proposed architecture is insensitive to the modulation format of the optically-carried RF input, we change it from CS-SSB modulation to double-sideband (DSB) modulation. The latter is very common in the optical communications. The RF signal is an LFM signal with an instantaneous bandwidth of 2 GHz centered at 13.5 GHz, and the LO has a frequency of 11.5 GHz. For the Hartley architecture, by injecting the RF signal and the corresponding image simultaneously, the mixing spur (2-6 GHz) overlaps with the desired IF signal (1-3 GHz), as shown in Fig. 9(a). The RF leakage (12.5-14.5 GHz) and the image leakage (8.5-10.5 GHz) with relatively high power can also be observed. Figure 9(b) shows the case when the proposed balanced Hartley architecture is applied. Again, a clean IF signal centered at 2 GHz with large suppression of the leakages and mixing spurs is obtained. Thus, the proposed balanced Hartley architecture can work well with different optical modulation format of the RF signal, which agrees well with the theory.
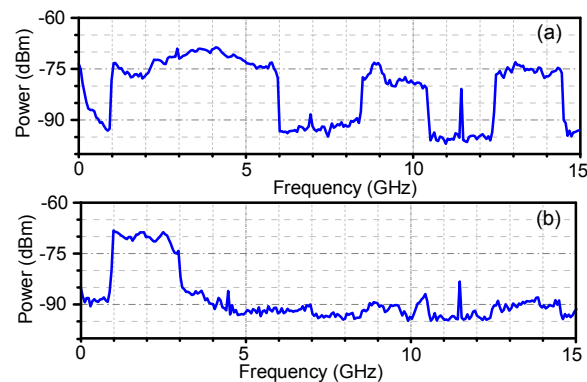

Fig. 9. The measured electrical spectra of the mixing results with an 11.5-GHz LO by injecting the RF signal (with a 2-GHz bandwidth centered at 13.5 GHz) and the image into the system simultaneously with the DSB modulation format for (a) the Hartley architecture and (b) the balanced Hartley architecture.

In order to further improve the system performance, feedback controlling circuits can be involved to adjust the phase shifts precisely. In addition, with the development of integrated photonic technologies, the performance can also be further improved by integrating the scheme into a chip.

4. Conclusion

In conclusion, we have proposed and demonstrated a novel architecture for broadband image-reject mixing which is uniquely enabled by photonic technology. As compared with the traditional Hartley or Weaver architecture, the proposed balanced Hartley architecture can reject the downconverted image, the RF/LO leakages and the nonlinear mixing spurs simultaneously. In an experiment, all these undesired components are suppressed by more than 60 dB over a 40-GHz working frequency range. In addition, a 6-dB improvement of the conversion efficiency is obtained by the proposed architecture. The concept can find applications in future wideband and multifunctional RF systems, including 5G and beyond wireless communications, ultrahigh-capacity satellite payloads, electronic warfare and multifunctional radars.

Funding

References

1. D. Onori, F. Scotti, F. Laghezza, M. Bartocci, A. Zaccaron, A. Tafuto, A. Albertoni, A. Bogoni, and P. Ghelfi, "A photonically enabled compact 0.5-28.5 GHz RF scanning receiver," J. Lightwave Technol. **36**(10), 1831–1839 (2018).
2. P. Ghelfi, F. Laghezza, F. Scotti, G. Serafino, A. Capria, S. Pinna, D. Onori, C. Porzi, M. Scaffardi, A. Malacarne, V. Vercesi, E. Lazzeri, F. Berizzi, and A. Bogoni, "A fully photonics-based coherent radar system," Nature **507**(7492), 341–345 (2014).
3. S. L. Pan, D. Zhu, S. F. Liu, K. Xu, Y. T. Dai, T. L. Wang, J. G. Liu, N. H. Zhu, Y. Xue, and N. J. Liu, "Satellite payloads pay off," IEEE Microw. Mag. **16**(8), 61–73 (2015).
4. B. Razavi, *RF Microelectronics*, II Edition (Pearson Education, 2012).
5. D. Zhu and S. L. Pan, "Photonics-based microwave image-reject mixer," MDPI Photon. **5**(2), 6 (2018).
6. H. Ogawa and H. Kamitsuna, "Fiber optic microwave links using balanced laser harmonic generation, and balanced/image cancellation laser mixing," IEEE Trans. Microw. Theory Tech. **40**(12), 2278–2284 (1992).
7. C. Lu, W. Chen, and J. F. Shiang, "Photonic mixers and image-rejection mixers for optical SCM systems," IEEE Trans. Microw. Theory Tech. **45**(8), 1478–1480 (1997).
8. J. Zhang, E. H. W. Chan, X. Wang, X. Feng, and B. Guan, "High conversion efficiency photonic microwave mixer with image rejection capability," IEEE Photonics J. **8**(4), 3900411 (2016).
9. Z. Z. Tang and S. L. Pan, "Image-reject mixer with large suppression of mixing spurs based on a photonic microwave phase shifter," J. Lightwave Technol. **34**(20), 4729–4735 (2016).
10. Y. Gao, A. Wen, W. Chen, and X. Li, "All-optical, ultra-wideband microwave I/Q mixer and image-reject frequency down-converter," Opt. Lett. **42**(6), 1105–1108 (2017).
11. W. Zhang, A. J. Wen, Y. S. Gao, S. Shang, H. X. Zheng, and H. Y. He, "Large bandwidth photonic microwave image rejection mixer with high conversion efficiency," IEEE Photonics J. **9**(3), 7201908 (2017).
12. Z. Tang and S. Pan, "Reconfigurable microwave photonic mixer with minimized path separation and large suppression of mixing spurs," Opt. Lett. **42**(1), 33–36 (2017).
13. Z. Z. Tang and S. L. Pan, "A reconfigurable photonic microwave mixer using a 90° optical hybrid," IEEE Trans. Microw. Theory Tech. **64**(9), 3017–3025 (2016).
14. Z. Meng, J. Li, C. Yin, Y. Fan, F. Yin, Y. Zhou, Y. Dai, and K. Xu, "Dual-band dechirping LFMCW radar receiver with high image rejection using microwave photonic I/Q mixer," Opt. Express **25**(18), 22055–22065 (2017).
15. Z. Shi, S. Zhu, M. Li, N. H. Zhu, and W. Li, "Reconfigurable microwave photonic mixer based on dual-polarization dual-parallel Mach-Zehnder modulator," Opt. Commun. **428**, 131–135 (2018).
16. W. J. Chen, D. Zhu and S. L. Pan, "Multi-octave image-reject mixer with large suppression of mixing spurs based on balanced photodetectors," in *CLEO 2018* (2018).
17. J. Capmany and D. Novak, "Microwave photonics combines two worlds," Nat. Photonics **1**(6), 319–330 (2007).